Journal of Asian Scientific Research
ISSN(e): 2223-1331
ISSN(p): 2226-5724
DOI: 10.55493/5003.v16i2.5897
Vol. 16, No. 2, 48-60.
© 2026 AESS Publications. All Rights Reserved.
URL: www.aessweb.com

Development of ZE41 Mg–Nano-CDHA composites for biodegradable implant applications

Katepalli Srivallirani[1]
Tapan Kumar Mahanta[2]
Kamaladevi Kolavennu[3]
Deepanraj Balakrishnan[4]
Ratna Sunil Buradagunta[5+]

[1]*Mechanical Engineering Department, M.B.T.S. Government Polytechnic, Guntur 522005, Andhra Pradesh, India.*
[1]*Email: srivalli.mech@gmail.com*
[2]*School of Mechanical Engineering, VIT University, Chennai-600127, India.*
[2]*Email: tapan.mahanta@vit.ac.in*
[3]*Department of Electrical and Electronics Engineering, Bapatla Engineering College, Bapatla 522101, Andhra Pradesh, India.*
[3]*Email: kamaladevi.bec@gmail.com*
[4,5]*Department of Mechanical Engineering, Prince Mohammad Bin Fahd University, Al-Khobar 31952, Kingdom of Saudi Arabia.*
[4]*Email: dbalakrishnan@pmu.edu.sa*
[5]*Email: rburadagunta@pmu.edu.sa*

(+ Corresponding author)

Article History
Received: 23 October 2025
Revised: 30 December 2025
Accepted: 3 February 2026
Published: 10 February 2026

Keywords
Biomaterial
Bone implants
Corrosion
Degradation
Friction stir processing
Hydroxyapatite
Mg composites
Nano-CDHA.

ABSTRACT

In this current work, nanocrystalline calcium-deficient hydroxyapatite (CDHA) was synthetically produced using calcium hydroxide and diammonium phosphate through a wet chemical synthesis route. X-ray diffraction (XRD) analysis and electron microscopy demonstrated the nano-level (~47 nm) of the produced CDHA. Then, the nano-CDHA was reinforced into ZE41 Mg alloy by friction stir processing (FSP) aimed at manufacturing degradable bone implants. Microstructures clearly demonstrated the development of a fine-grained structure (7.4 ± 6.9 µm) in addition to incorporating nano-CDHA into ZE41 Mg alloy. FSP resulted in decreased intermetallic phases, which suggests increased solubility of zinc into magnesium due to FSP. XRD analysis of the composite confirms the development of a basal-dominated texture in the composite. From the potentiodynamic polarization studies, corrosion performance was assessed using simulated body fluid (SBF). The composite exhibited noble behavior by demonstrating a lower corrosion current density (-1.23 ± 0.8 × 10^{-4} A/cm^2) compared with ZE41 alloy (-4.75 ± 1.1 × 10^{-4} A/cm^2). Lower weight loss was observed for the composite after 72 hours of immersion in SBF, indicating improved degradation resistance due to the incorporated nano-CDAH and grain refinement. The lower corrosion rate measured for the composite (11.4 ± 2.1 mm/year) is 40% lower compared with ZE41 alloy (19.3 ± 1.8 mm/year) based on weight loss data. The results demonstrate the feasibility of FSP to develop ZE41-nano-CDHA composite with better corrosion control.

Contribution/ Originality: The paper's primary contribution is the development of a novel composite of ZE41-nano-CDHA through friction stir processing, aimed at manufacturing magnesium-based implants for medical applications. The results demonstrate the promising role of a refined microstructure and the addition of nano-CDHA to the ZE41 alloy in enhancing degradation resistance.

1. INTRODUCTION

Developing magnesium (Mg)-based composites for degradable implant applications has become a significant area of research in the field of material science [1, 2]. Using nano-phases as reinforcements in various Mg alloys to tailor the degradation rate, bioactivity, biomineralization, and implant-tissue interactions is extensively documented in

© 2026 AESS Publications. All Rights Reserved.

recent literature [3]. Among the potential reinforcements, calcium-based phases are the most promising for developing magnesium-based composites [4, 5]. Among the available Mg alloys, ZE41 Mg alloy, which contains zinc and rare earth elements as the principal alloying elements, has recently been considered a promising material for implants.

In addition to incorporating biocompatible phases into Mg alloys, modifying the microstructure is another potential strategy employed to enhance the properties of Mg alloys [6]. Friction stir processing (FSP) is a solid-state method that can be successfully used to refine the microstructure of Mg alloys [7-9]. It was demonstrated that the fine grain structure produced in ZE41 Mg alloy by FSP helps to increase strength and corrosion resistance [10]. Using hydroxyapatite as a reinforcing phase to develop magnesium-based composites through friction stir processing (FSP), with enhanced bio-properties, can be observed from the literature [11-13]. By decreasing the calcium (Ca) content, calcium-deficient hydroxyapatite (CDHA) can be produced [14, 15]. Ca to P ratio in CDHA is usually observed as less than 1.67 [16, 17]. Hydroxyapatite is stable in the bio-environment, whereas the stability of CDHA is inferior, and it degrades slowly in the bio-environment [18, 19]. Since the objective behind producing Mg-based implants is for temporary applications, using degradable CDHA phases to develop Mg composites is appropriate. Very recently, AZ31 Mg alloy was incorporated with CDHA, and increased biomineralization was observed in the composites [20]. The information on using nano-CDHA as reinforcement to produce Mg-based implants is insufficient in the literature. Furthermore, using nano-CDHA to produce composites of ZE41 alloy has not yet been explored. Therefore, in the current research work, nano-CDHA powder was produced by a wet chemical synthesis method, and using FSP, composites of ZE41-nano-CDHA were produced with the objective of investigating the composite for degradable implant applications. The literature related to the current research work, details of the experiments, data collection and analysis methods, and discussion of the obtained results, followed by conclusions, are presented in the following sections.

2. LITERATURE

From the earlier literature, developing Mg composites by dispersing HA can be seen as a potential strategy to impart higher performance in Mg implants. The first benefit of the addition of HA is the increased bioactivity [21]. Increased biomineralization and controlled degradation are the other advantages associated with HA [22]. Due to the dispersion strengthening mechanism, the addition of HA also contributes to increasing the mechanical properties of Mg composites [23]. However, it was also reported that a higher amount of HA causes galvanic corrosion and localized corrosion, which leads to a decrease in corrosion resistance [24]. Furthermore, higher amounts of HA lead to agglomeration and increase the brittleness of Mg composites [25]. Therefore, the selection of the fraction of HA that is added to Mg and its alloys to develop composites with enhanced performance is crucial in designing medical implants for temporary degradable applications. Table 1 presents a brief summary of the earlier reported works in producing Mg-based composites dispersed with HA for degradable implant applications.

Table 1. A brief summary of Mg-HA composites developed for biomedical applications.

S.No.	Composite	Process	Significant findings	Reference
1	AZ91/HA	Hot extrusion	• Adding HA crystals induced controlled and uniform corrosion • The surfaces were observed with $CaCO_3$ phases in the immersion studies	Witte, et al. [26]
2	Mg-Ca/HA-TCP	Liquid alloy infiltration	• Excellent corrosion resistance in Hank's solution • Cell viability tests indicated grade-1 toxicity towards L-929 and MG63 cells.	Gu, et al. [27]
3	Mg/HA-MgO	Blend-cold press-sinter	• Higher corrosion resistance was achieved for the Mg/12.5HA/10MgO composition. • Excellent cell response against osteoblast cells	Khalajabadi, et al. [28]

© 2026 AESS Publications. All Rights Reserved.

S.No.	Composite	Process	Significant findings	Reference
4	Mg-HA	FSP	• Enhanced corrosion resistance in simulated physiological solutions. • Higher biomineralization due to grain refinement. • Improved cell viability and cell adhesion	Sunil, et al. [21]
5	Mg-HA, AZ91/HA	Quasi-constrained HPT	• Decreased corrosion rate and higher cell viability have been observed for the Mg-HA composite. •	Castro, et al. [29]
6	Mg-HA	Spark plasma sintering	• Better properties were observed when the porosity was less than 1.9%. • Increased corrosion resistance and compressive strength • Formation of MgO due to the oxidation of Mg during synthesis was also observed, which decreased the compressive strength.	Nakahata, et al. [23]
7	ZK60/HA	Powder metallurgy	• Better wear-corrosion resistance was achieved at 10% HA addition • Corrosion and abrasion are the main mechanisms for the material loss for the composites in the SBF	Su, et al. [30]
8	Mg-HA	Rapid microwave sintering	• Layered composites exhibited increased microhardness and compressive strength. • From the immersion tests conducted at SBF, improved corrosion resistance was observed for the composite.	Shamami, et al. [31]
9	Mg/HA Mg-3Al/HA	Material extrusion additive manufacturing	• Compared with Mg-Al, when Mg was used as the matrix material, the addition of HA has shown a significant effect on improving the strength. • From the immersion studies, poor corrosion resistance was observed in the composites due to galvanic corrosion.	Casas-Luna, et al. [32]
10	Mg-Zn/HA	Ball milling -cold pressing	• Lower HA content resulted in reduced porosity and enhanced mechanical performance and corrosion resistance. • Lower amounts of HA are advised to attain improved mechanical performance and corrosion resistance.	Lu, et al. [25]
11	Mg-HA	Electromagnetic and mechanical stir casting	• The composite subjected to 4-pass ECAP resulted in grain size reduction and uniform microstructure • Higher tensile strength and fracture strength were reported for the ECAPed composite.	Kasaeian-Naeini, et al. [33]
12	WE43/HA	FSP	• Improved yield strength and ultimate tensile strength (UTS) were observed, resulting from the refined microstructure. • Presence of HA decreased the corrosion rate up to 30%.	Wang, et al. [4]
13	WE43/HA	Additive manufacturing	• The scaffolds with 70% porosity were successfully produced, and the composite scaffolds exhibited a higher compressive strength (180%).	Drotárová, et al. [34]
14	Mg-HA	Spark plasma sintering	• Applying PLC coating on the composite reduced the corrosion rate by up to threefold. • Long-term immersion in 0.9% NaCl exhibited lower degradation for the composites with PLC.	Podgorbunsky, et al. [35]
15	Mg-nanodiamond/HA	3D printing	• Composites exhibited excellent strength and fracture resistance. • Cell culture studies utilizing human mesenchymal stem cells demonstrated higher cell adhesion.	Acharya, et al. [36]

© 2026 AESS Publications. All Rights Reserved.

S.No.	Composite	Process	Significant findings	Reference
16	Mg/HA, Mg-Zn/HA, Mg-Sn/HA	ultrasonic-assisted rheo-casting technology	• Mg-Sn/HA composite has demonstrated the highest hardness (94.8 HV) among all the composites, primarily due to precipitation. • Mg-Zn/HA composite exhibited lower degradation (0.19 mm/year) due to the uniform distribution of HA and a refined microstructure. • The Mg-Zn/HA composite demonstrated higher cell viability against MG-63 cells, attributed to increased biomineralization.	Narayanappa, et al. [37]

From the available literature, it can be learned that adding hydroxyapatite (HA) to magnesium (Mg) and its alloys enhances their mechanical properties and corrosion resistance. However, some reports also demonstrate decreased corrosion performance in Mg composites reinforced with HA, primarily due to galvanic corrosion [33, 38]. Adding lower amounts of HA was observed to be promising, as it helps avoid limitations such as agglomeration, galvanic corrosion, and decreased fracture toughness [25]. Using nano-crystalline hydroxyapatite (HA) also presents a potential strategy to enhance the mechanical properties and corrosion resistance of magnesium-hydroxyapatite (Mg-HA) composites [22, 25]. However, it can be learned that information on developing ZE41-CDHA composites by FSP for biodegradable implant applications is lacking. Furthermore, reinforcing CDHA into ZE41 Mg alloy and its effect on mechanical and corrosion properties have not yet been explored, which is the main objective of the current research work.

3. METHODOLOGY

3.1. Synthesizing Nano-CDHA

Nano-CDHA was synthesized by using $Ca(OH)_2$ (calcium hydroxide, Merck, USA) and $(NH_4)_2HPO_4$ (diammonium phosphate, Merck, USA). Aqueous solutions were prepared using deionized water. To achieve a lower Ca/P ratio (1.5), 1 M solutions of both precursors were prepared and mixed in appropriate ratios using a magnetic stirrer. $Ca(OH)_2$ aqueous solution was added into a beaker, and the solution of $(NH_4)_2HPO_4$ was added drop by drop while the solution was continuously stirred. By adding ammonia to the solution drop by drop, the pH of the solution in the beaker was maintained above 9 to avoid any precipitations during the synthesizing process. After completely mixing the solutions, stirring was done for 1 hour, and then the beaker was placed in a hot oven to allow the precipitation. The precipitated powder was then collected from the beaker, crushed, and filtered using deionized water through filter papers, and the leftover powder was collected.

3.2. Producing ZE41-CDHA Composites

Composites of ZE41 Mg alloy with nano-CDHA were produced by FSP. Figure 1 illustrates the process of developing composites by FSP and a typical photo obtained during the process. Initially, a groove (2 mm depth with 1 mm width) was produced on the ZE41 workpiece by a milling cutter and then filled with nano-CDHA. It was ensured that the groove was filled with 70% tap density. The CDHA-filled groove was then processed with a pin-less flat surface tool to constrain the CDHA within the groove. An FSP tool with a tapered circular pin of 6 mm length, with diameters varying from 5 mm to 2 mm, was used for a single pass by selecting process parameters (1400 rpm speed with 25 mm/min feed) based on the literature [20]. From the cross-sectional observations, a defect-free stir zone was observed. The samples for characterization and studies were collected from the center of the produced composites.

© 2026 AESS Publications. All Rights Reserved.

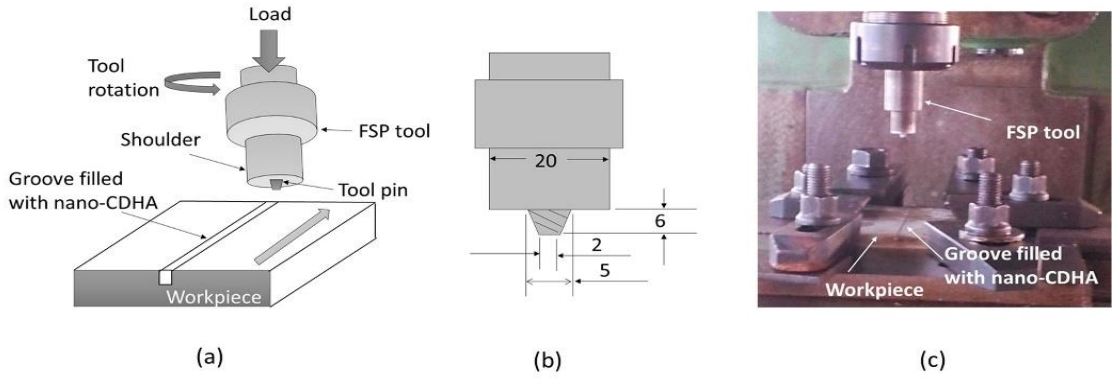

Figure 1. (a) Schematic presentation of FSP of ZE41-nano-CDHA composite, (b) tool dimensions, and (c) photograph obtained during the process.

3.3. Characterization

The produced nano-CDHA powder, base alloy, and the composite were characterized by X-ray diffraction (XRD, Bruker, USA) from 20° to 80° range with a step size of 0.1° using CuKα radiation. All the peaks in the XRD were matched with the International Centre for Diffraction Data (ICDD) and indexed. Transmission electron microscopy (HR-TEM, Philips, Holland) was performed to study the morphology of the CDHA powders, and the corresponding electron diffraction pattern was also obtained.

For microstructural studies, a standard metallographic polishing process was adopted. For polishing, different graded emery sheets were used, followed by diamond paste (1-3 µm particle size) and lubricant on a rotating disc polishing machine. The surfaces were then etched with an etchant composed of 50 ml of ethanol, 2.5 ml of picric acid, 2.5 ml of acetic acid, and 2.5 ml of distilled water. Etching was performed for 20 s, then dried in open air before observing the microstructures. The micrographs were obtained for the base alloy (ZE41) and the composite (ZE41-nano-CDHA) using a Leica optical microscope, Germany.

3.4. Corrosion Studies by Potentiodynamic Polarization

Corrosion studies were conducted using simulated body fluid (SBF). The preparation method and the ion concentration of SBF can be referenced elsewhere [39]. SBF closely resembles human body fluid and contains a similar ion concentration. For potentiodynamic polarization studies (IVIUM Soft, Netherlands), the workpiece surface (1 cm^2) was exposed to the corrosive electrolyte within the corrosion test cell. Tests were performed in the presence of a platinum rod and a saturated calomel electrode. The scanning was conducted at a rate of 5 mV/s, and from the data obtained, Tafel extrapolation was used to determine the electrochemical parameters [38].

3.5. Degradation Behavior by Immersion Studies

The samples (10 × 10 × 2 mm^3) were immersed in SBF for 24 h, 48 h, and 72 h at 37 °C in a temperature-controlled water bath to assess weight loss. The collected samples from the SBF were then gently washed in de-ionized water and placed in CrO_3 solution (180 g per 1 liter of water) to dissolve the corrosion products. The weights before and after immersion studies were measured, and the weight loss of the samples due to biodegradation in SBF was compared. The corrosion rate (CR) in mm/year was obtained from the data in Equation 1 [40].

$$CR\ (mm/year) = (8.76 \times 10^4 \times w) / (A.\ t.\ \rho) \quad (1)$$

Where w is weight loss (g), A is the surface area of the sample (cm^2), t is immersion time (h), and ρ is the density (g/cm^3).

© 2026 AESS Publications. All Rights Reserved.

3.6. Statistical Analysis

All the experiments were conducted in triplicate (n=3). From the obtained data, mean values were calculated, and the standard deviation values were obtained. The statistical analysis was carried out using the one-way ANOVA method with OriginPro8 software (USA). A p-value of less than 0.05 was considered statistically significant.

4. RESULTS AND DISCUSSION

The characterization of the produced nano-CDHA was done by XRD, as presented in Figure 2. All the peaks were indexed by referring to standard data (ICDD, JCPDS no. 09-0432). By measuring the peak (002) width at half of the peak height, the crystallite size was calculated as 47 nm for the produced nano-CDHA using Scherrer's formula [41]. From the XRD analysis, it is confirmed that the CDHA is at the nano-level. Adding nano-crystalline reinforcements to Mg helps increase mechanical performance and corrosion properties. Agglomeration is an issue with nano-crystalline materials. However, it has been reported that FSP can reduce the agglomeration issue, as the material stirring during FSP helps to distribute the reinforcements uniformly in the matrix [4, 21]. However, because of the higher surface energy of nanocrystalline materials, agglomeration can be observed in FSPed composites also up to some levels. Compared with liquid state methods, where agglomeration of nano-reinforcements is a serious concern, FSP results in a lower level of agglomeration, which is beneficial. The TEM bright field image of the powder and the corresponding electron diffraction pattern are presented in Figure 3. It is noted that the nano-CDHA crystals are showing acicular morphology with varying thickness-to-length ratios. The nano-size of the crystals is confirmed from the images, as understood from the XRD analysis. The electron diffraction pattern appears as a spot pattern in ring-like morphology, also reflecting the nano-level of the produced CDHA. Both the TEM studies and XRD data are in good agreement, demonstrating the nano-level of the CDHA. Compared with spherical morphology, acicular morphology in CDHA increases the surface area of the CDHA crystals and enhances the bonding between the CDHA crystals and the matrix, as reported by Siva Krishna and Suresh in developing HA-incorporated Ti-HA composites [42].

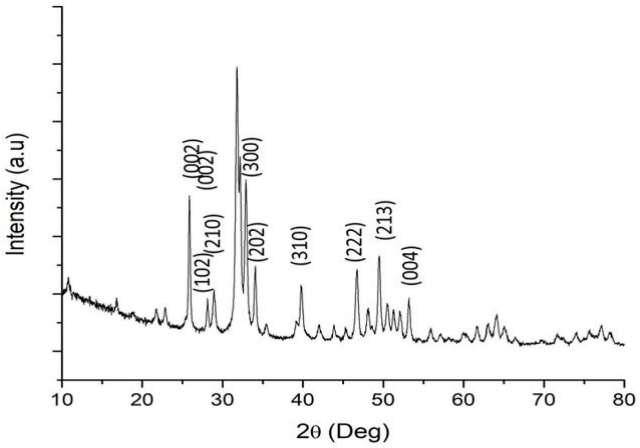

Figure 2. XRD pattern of nano-CDHA produced in the present work.

The microstructures of ZE41 and ZE41-nano-CDHA samples are presented in Figure 4. The microstructure of ZE41 (Figure 4 (a)) clearly shows the average grain size as 102 ± 9.5 μm. Additionally, the presence of intermetallic phases at the grain boundaries can also be clearly seen as a network structure. Usually, in ZE41 Mg alloy, MgZn intermetallics (as indicated with white arrows) are widely observed at room temperature. The microstructure of the ZE41-nano-CDHA sample clearly shows the evolution of smaller grains (7.4 ± 6.9 μm) due to FSP. Typically, in FSP, dynamic recrystallization produces a fine-grain structure [6]. Additionally, the amount of intermetallic was observed to have decreased clearly from the ZE41-nano-CDHA microstructure. Agglomerates of CDHA were also observed in the composites (indicated with arrows) in Figure 4 (b). Due to the nano-size of the CDHA, the incorporated particles

© 2026 AESS Publications. All Rights Reserved.

were found to be agglomerated in some regions of the composite. This is similar to earlier findings, where when nanophases were dispersed by FSP, agglomeration was a common observation [4, 21]. Since the objective of adopting FSP is to incorporate nano-CDHA into ZE41 to achieve the benefits from the presence of a degradable Ca-based phase to tailor the bio-properties for implant applications, the observed minimal agglomeration is less concerning.

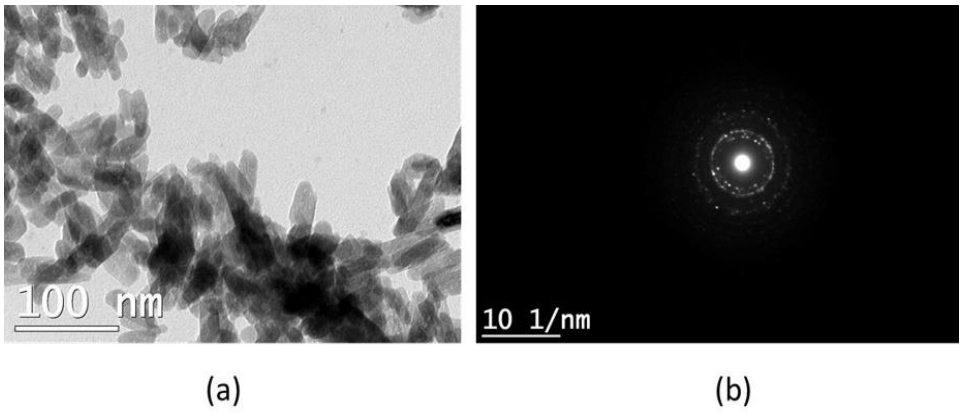

Figure 3. (a) TEM image and (b) electron diffraction pattern of nano-CDHA.

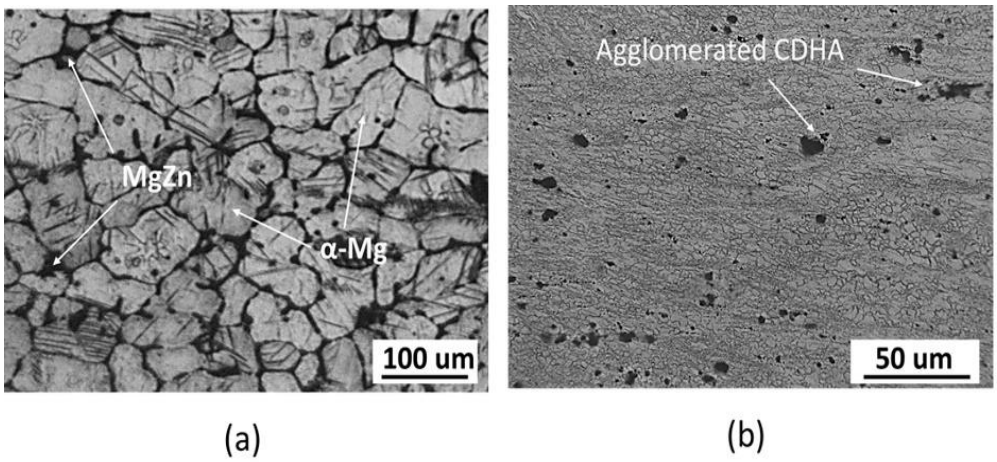

Figure 4. Microstructures of (a) ZE41 and (b) ZE41-nanoCDHA composite.

Figure 5 presents the XRD analysis of ZE41 and ZE41-nanoCDHA samples. All the peaks were indexed. No peaks other than α-Mg were noticed in the XRD plot. Due to the smaller amount of intermetallic phase in the base alloy, the corresponding peaks were not identified. The intensities of peaks in the ZE41-nano-CDHA sample were significantly altered. The intensities of (100), (101), and (102) were significantly decreased, and the intensities of (002), (103), and (004) were significantly increased after FSP. This behavior clearly indicates the texture effect in the produced composite. Particularly, the intensity of the (002) peak (high-density plane) has been significantly increased, suggesting the development of a basal-dominated texture in the composite. Surprisingly, from the XRD plot of the composite, peaks corresponding to nano-CDHA were not identified due to the presence of the reinforcement in the sample within the lower limits of detection in XRD. From microstructural studies and XRD analysis, the composite was identified with three major microstructural modifications: i. grain refinement, ii. decreased intermetallic phase, and iii. basal-dominated texture. These three factors greatly influence the corrosion behavior of the developed composite.

© 2026 AESS Publications. All Rights Reserved.

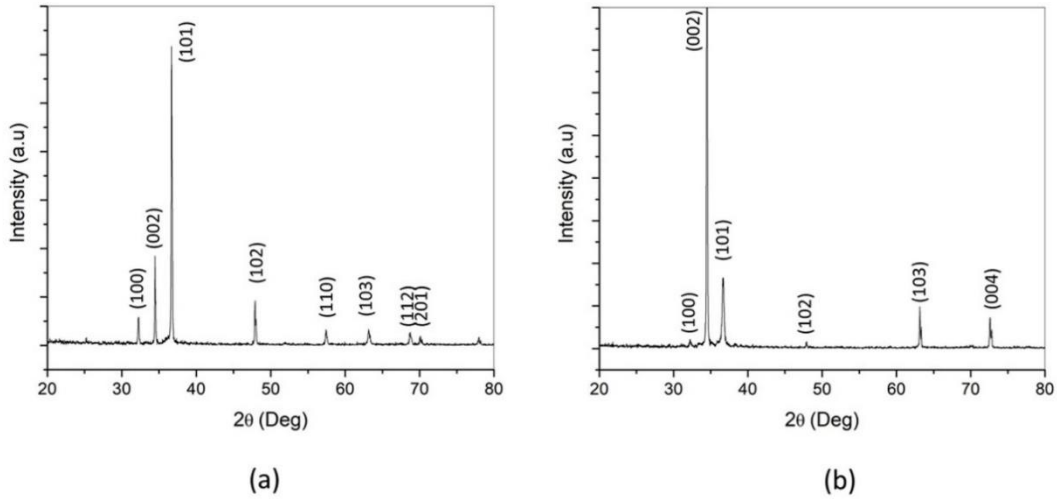

Figure 5. XRD patterns of the samples: (a) ZE41 and (b) ZE41-nanoCDHA.

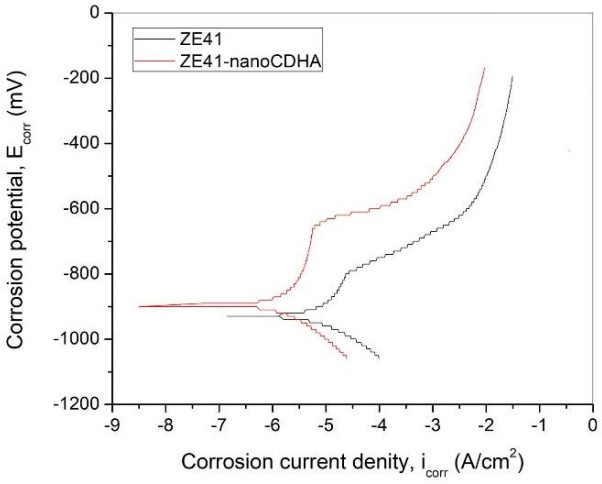

Figure 6. PDP curves of the samples.

Table 2. Corrosion parameters obtained from the PDP curves.

Sample	Corrosion parameters	
	Potential (E_{corr}), mV	Current density (i_{corr}), A/cm²
ZE41	-929 ± 55	$-4.75 \pm 1.1 \times 10^{-4}$
ZE41-nano-CDHA	-890 ± 39	$-1.23 \pm 0.8 \times 10^{-4}$

Figure 6 shows the PDP curves drawn from the electrochemical studies. From the Tafel extrapolation, corrosion parameters (E_{corr} and i_{corr}) were obtained and presented in Table 2. Composite exhibited noble behavior as reflected by the potential shift towards positive values compared with ZE41. From the i_{corr} values, a lower value was observed for the ZE41-nano-CDHA compared with ZE41, which indicates lower electrochemical activity for the composite. Lower i_{corr} values obtained for the composite indicate higher corrosion resistance for the composite. From the works of Chun, et al. [43] it can be understood that the addition of HA (0.5%) to Mg-Zn-Y alloy improved the corrosion resistance, as reflected in lower i_{corr} values (118.63 µA/cm²) measured from the PDP studies. It was also reported by Jaiswal, et al. [44] that at the lower amount of HA (2% and 5% by weight), decreased i_{corr} values (777.02 ± 3.77 µA/cm² and 571.97 ± 4.17 µA/cm²) were observed for Mg-3Zn-HA composites prepared by conventional sintering. With the higher HA content, the i_{corr} values increased again (682.16 ± 4.97 µA/cm²) due to galvanic corrosion. In the present work, ZE41-HA composite produced by FSP showed marginally lower i_{corr} values, suggesting the potential of refined microstructure and the addition of HA by FSP in improving corrosion resistance.

© 2026 AESS Publications. All Rights Reserved.

On the other hand, Mg-5Zn alloy subjected to FSP at different process parameters exhibited i_{corr} values ranging from 1103.5 μA/cm² to 11.8 μA/cm² when the FSP tool speed increased from 800 rpm to 1000 rpm, and then increased to 806.7 μA/cm² when the tool speed was increased to 1250 rpm [45]. By observing the reported i_{corr} values in connection with Mg-Zn-based biomaterials, the i_{corr} values obtained in the present work are promising.

Table 3. Weight loss measurements of the samples.

Sample	Weight loss after immersion (%)		
	24 h	48 h	72 h
ZE41	5.39 ± 0.99	11.16 ± 1.7	15.73 ± 1.69
ZE41-nano-CDHA	4.8 ± 1.04	7.13 ± 0.72	9 ± 1.32

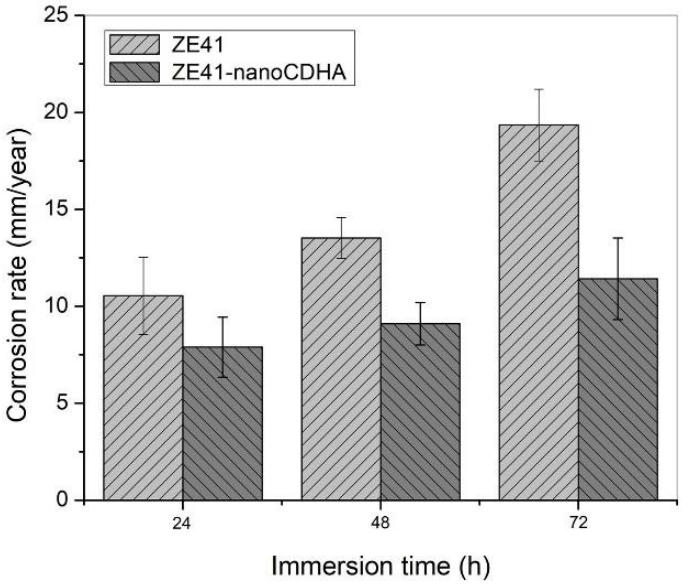

Figure 7. The corrosion rate of the samples was calculated from the weight loss measurements.

The weight loss measurements, considering the initial weight and the remaining weight of the samples after immersion tests, are presented in Table 3. The corrosion rate of the sample was calculated and compared in Figure 7. Lower weight loss was observed for the composites at all immersion times compared with ZE41. The corrosion rate increased with immersion time for ZE41 and ZE41-nano-CDHA. However, ZE41-nano-CDHA exhibited a lower corrosion rate than ZE41 after 24 h, 48 h, and 72 h of immersion. Corrosion experiments from PDP tests and immersion tests demonstrate a decreased corrosion rate for ZE41-nano-CDHA. The microstructure refinement and the incorporated nano-CDHA by FSP have a profound effect on decreasing the corrosion rate of the composite. The produced smaller grains initiate the development of a quick passive film, $Mg(OH)_2$ in Mg alloys, which protects against further corrosion [46]. The addition of nano-CDHA helped to decrease the corrosion rate in the ZE41-nano-CDHA. Basal-dominated texture in Mg-based composites decreases the corrosion rate [47, 48]. The combined effect of these factors contributed to improved corrosion resistance in the produced ZE41-nano-CDHA.

Similar improvements in corrosion resistance were reported in developing Mg-based composites targeted for implant applications. Reinforcing Ca-based phases promotes bioactivity and biomineralization in Mg alloys, which enhances the healing rate when used as candidates to manufacture orthopedic implants [49, 50]. In the present work, using degradable nano-CDHA helps to control degradation and also promotes improved tissue-implant bonding by enhancing bioactivity. Furthermore, compared with stable HA, nano-CDHA gradually degrades along with the Mg alloy in the physiological environment and leaves no traces at the site of new bone formation. The current study demonstrates the promising behavior of ZE41-nano-CDHA as an implant material for manufacturing degradable bone fixing plates and scaffolds. The distribution of nano-phases is challenging in FSP when producing the

© 2026 AESS Publications. All Rights Reserved.

composites. To address the agglomeration issue and to distribute nano-CDHA into ZE41 alloy, multi-pass FSP can be adopted.

5. CONCLUSIONS

5.1. Implications

Nano-CDHA was synthesized by a wet chemical method as a potential reinforcing phase to incorporate into ZE41 Mg alloy to produce a degradable composite by friction stir processing. The produced CDHA powder was characterized at the nano level using XRD and TEM analysis. The produced composites exhibit significant grain refinement. Additionally, a basal-dominated texture can be successfully produced in the composite, as characterized by XRD analysis. Due to the refined microstructure and the added CDHA, increased corrosion resistance can be achieved in the composites, as confirmed by PDP tests. Lower weight loss can be achieved in the presence of a physiological environment, as assessed indirectly from the immersion tests carried out in SBF. The corrosion rate calculated from the data exhibits a lower corrosion rate for the composites due to the produced smaller grain size, texture effect, and the incorporated nano-CDHA. The results demonstrate the feasibility of developing ZE41-nano-CDHA composite by FSP with enhanced corrosion resistance for degradable bone implant applications.

5.2. Limitations

The uniformity in dispersion of CDHA into ZE41 is challenging due to its nano-size. Even though the FSP method results in a lower level of agglomeration compared with liquid state methods, there is still a need to optimize the process parameters to achieve a higher level of uniformity in the dispersion of CDHA. The size of the produced composite is limited to the width of the FSP tool shoulder, and hence, additional parallel passes are required to develop components in larger dimensions.

5.3. Future Research Suggestions

In order to achieve improved uniformity in the dispersion of nano-CDAH, carrying out multi-pass FSP to study the effect of the number of passes on altering the distribution of CDHA into ZE41 is needed, which can be a part of the future scope. On the other hand, the longer degradation behavior and its effect on mechanical failure in the presence of corrosion cracks also need to be evaluated. Additionally, investigating the toxicity of the composite against appropriate cell lines and the impact of the degradation process on cell activities can also be carried out as part of the future scope of the work to make ZE41-nano-CDHA composites produced by FSP a viable material for manufacturing degradable medical implants.

Funding: This study received no specific financial support.
Institutional Review Board Statement: Not applicable.
Transparency: The authors state that the manuscript is honest, truthful, and transparent, that no key aspects of the investigation have been omitted, and that any differences from the study as planned have been clarified. This study followed all writing ethics.
Competing Interests: The authors declare that they have no competing interests.
Authors' Contributions: All authors contributed equally to the conception and design of the study. All authors have read and agreed to the published version of the manuscript.

REFERENCES

[1] J.-L. Wang, J.-K. Xu, C. Hopkins, D. H.-K. Chow, and L. Qin, "Biodegradable magnesium-based implants in orthopedics—a general review and perspectives," *Advanced Science*, vol. 7, no. 8, p. 1902443, 2020. https://doi.org/10.1002/advs.201902443

[2] Y. Luo, J. Wang, M. T. Y. Ong, P. S.-H. Yung, J. Wang, and L. Qin, "Update on the research and development of magnesium-based biodegradable implants and their clinical translation in orthopaedics," *Biomaterials Translational*, vol. 2, no. 3, pp. 188–196, 2021. https://doi.org/10.12336/biomatertransl.2021.03.003

© 2026 AESS Publications. All Rights Reserved.

[3] H. Guan *et al.*, "A review of the design, processes, and properties of Mg-based composites," *Nanotechnology Reviews*, vol. 11, no. 1, pp. 712–730, 2022. https://doi.org/10.1515/ntrev-2022-0043

[4] X. Wang *et al.*, "Fabrication of high-performance biomedical rare-earth magnesium alloy-based WE43/hydroxyapatite composites through multi-pass friction stir processing," *Journal of Materials Research and Technology*, vol. 33, pp. 5349-5363, 2024. https://doi.org/10.1016/j.jmrt.2024.10.060

[5] Y.-H. Tsai *et al.*, "Novel artificial tricalcium phosphate and magnesium composite graft facilitates angiogenesis in bone healing," *Biomedical Journal*, vol. 48, no. 2, p. 100750, 2025. https://doi.org/10.1016/j.bj.2024.100750

[6] G. Li *et al.*, "Development of biodegradable Mg–Zn alloys by grain refinement through extrusion," *The Journal of The Minerals, Metals & Materials Society*, vol. 77, no. 6, pp. 4384–4392, 2025. https://doi.org/10.1007/s11837-025-07177-6

[7] Z. Y. Ma, "Friction stir processing technology: A review," *Metallurgical and Materials Transactions A*, vol. 39, no. 3, pp. 642-658, 2008. https://doi.org/10.1007/s11661-007-9459-0

[8] W. Wang *et al.*, "Friction stir processing of magnesium alloys: A review," *Acta Metallurgica Sinica (English Letters)*, vol. 33, no. 1, pp. 43–57, 2020. https://doi.org/10.1007/s40195-019-00971-7

[9] R. V. Marode, T. A. Lemma, N. Sallih, S. R. Pedapati, M. Awang, and A. Hassan, "Research progress in friction stir processing of magnesium alloys and their metal matrix surface composites: evolution in the 21st century," *Journal of Magnesium and Alloys*, vol. 12, no. 6, pp. 2091-2146, 2024. https://doi.org/10.1016/j.jma.2024.06.007

[10] V. S. S. H. Vardhan and A. Sharma, "Investigating the degradation behavior of grain refined WE43 magnesium alloy produced by friction stir processing for medical implant applications," *Journal of Mines, Metals & Fuels*, vol. 71, no. 12, pp. 2805–2813, 2023. https://doi.org/10.18311/jmmf/2023/41614

[11] E. Moradi, M. Ebrahimian-Hosseinabadi, M. Khodaei, and S. Toghyani, "Magnesium/nano-hydroxyapatite porous biodegradable composite for biomedical applications," *Materials Research Express*, vol. 6, no. 7, p. 075408, 2019. https://doi.org/10.1088/2053-1591/ab187f

[12] A. Dubey, S. Jaiswal, A. Garg, V. Jain, and D. Lahiri, "Synthesis and evaluation of magnesium/co-precipitated hydroxyapatite based composite for biomedical application," *Journal of the Mechanical Behavior of Biomedical Materials*, vol. 118, p. 104460, 2021. https://doi.org/10.1016/j.jmbbm.2021.104460

[13] S. Dutta, S. Gupta, and M. Roy, "Recent developments in magnesium metal–matrix composites for biomedical applications: A review," *ACS Biomaterials Science & Engineering*, vol. 6, no. 9, pp. 4748–4773, 2020. https://doi.org/10.1021/acsbiomaterials.0c00678

[14] V. P. Orlovskii, V. S. Komlev, and S. M. Barinov, "Hydroxyapatite and hydroxyapatite-based ceramics," *Inorganic Materials*, vol. 38, no. 10, pp. 973-984, 2002. https://doi.org/10.1023/A:1020585800572

[15] B. Viswanath, V. V. Shastry, U. Ramamurty, and N. Ravishankar, "Effect of calcium deficiency on the mechanical properties of hydroxyapatite crystals," *Acta Materialia*, vol. 58, no. 14, pp. 4841-4848, 2010. https://doi.org/10.1016/j.actamat.2010.05.019

[16] Z. Yuan *et al.*, "A novel synthesis method and properties of calcium-deficient hydroxyapatite/α-TCP biphasic calcium phosphate," *Journal of Biomaterials Applications*, vol. 36, no. 9, pp. 1712-1719, 2022. https://doi.org/10.1177/08853282211068597

[17] Y. W. Sari, A. Tsalsabila, N. Darmawan, and Y. Herbani, "Hydroxyapatite formation under calcium-deficient concentration conditions modulated by amino acid-capped gold nanoparticles," *Ceramics International*, vol. 48, no. 10, pp. 13665-13675, 2022. https://doi.org/10.1016/j.ceramint.2022.01.247

[18] Y. Hu *et al.*, "Enhanced reparative dentinogenesis of biphasic calcium phosphate ceramics containing calcium-deficient hydroxyapatite (CDHA) and strontium-incorporated CDHA in direct pulp capping," *Materials Today Communications*, vol. 33, p. 104231, 2022. https://doi.org/10.1016/j.mtcomm.2022.104231

[19] M. Lakrat, H. Jodati, E. M. Mejdoubi, and Z. Evis, "Synthesis and characterization of pure and Mg, Cu, Ag, and Sr doped calcium-deficient hydroxyapatite from brushite as precursor using the dissolution-precipitation method," *Powder Technology*, vol. 413, p. 118026, 2023. https://doi.org/10.1016/j.powtec.2022.118026

© 2026 AESS Publications. All Rights Reserved.

[20] K. E. Manoj, P. S. Kishore, and S. B. Ratna, "AZ31-calcium-deficient hydroxyapatite (CDHA) composites produced by friction stir processing: Controlling the degradation by enhancing the biomineralisation," *Canadian Metallurgical Quarterly*, vol. 64, no. 1, pp. 248–259, 2025. https://doi.org/10.1080/00084433.2024.2351346

[21] B. R. Sunil, T. S. S. Kumar, U. Chakkingal, V. Nandakumar, and M. Doble, "Friction stir processing of magnesium–nanohydroxyapatite composites with controlled in vitro degradation behavior," *Materials Science and Engineering: C*, vol. 39, pp. 315-324, 2014. https://doi.org/10.1016/j.msec.2014.03.004

[22] Y.-H. Ho *et al.*, "In-vitro biomineralization and biocompatibility of friction stir additively manufactured AZ31B magnesium alloy-hydroxyapatite composites," *Bioactive Materials*, vol. 5, no. 4, pp. 891-901, 2020. https://doi.org/10.1016/j.bioactmat.2020.06.009

[23] I. Nakahata, Y. Tsutsumi, and E. Kobayashi, "Mechanical properties and corrosion resistance of magnesium–hydroxyapatite composites fabricated by spark plasma sintering," *Metals*, vol. 10, no. 10, p. 1314, 2020. https://doi.org/10.3390/met10101314

[24] R. Radha and D. Sreekanth, "Mechanical and corrosion behaviour of hydroxyapatite reinforced Mg-Sn alloy composite by squeeze casting for biomedical applications," *Journal of Magnesium and Alloys*, vol. 8, no. 2, pp. 452-460, 2020. https://doi.org/10.1016/j.jma.2019.05.010

[25] W. Lu, Y. Zhang, and T. Wang, "Microstructure, mechanical properties, in vitro biodegradability, and biocompatibility of Mg-Zn/HA composites for biomedical implant applications," *Materials*, vol. 16, no. 16, p. 5669, 2023. https://doi.org/10.3390/ma16165669

[26] F. Witte *et al.*, "Biodegradable magnesium–hydroxyapatite metal matrix composites," *Biomaterials*, vol. 28, no. 13, pp. 2163-2174, 2007. https://doi.org/10.1016/j.biomaterials.2006.12.027

[27] X. N. Gu, X. Wang, N. Li, L. Li, Y. F. Zheng, and X. Miao, "Microstructure and characteristics of the metal–ceramic composite (MgCa-HA/TCP) fabricated by liquid metal infiltration," *Journal of Biomedical Materials Research Part B: Applied Biomaterials*, vol. 99, no. 1, pp. 127-134, 2011. https://doi.org/10.1002/jbm.b.31879

[28] S. Z. Khalajabadi, M. R. A. Kadir, S. Izman, and M. Marvibaigi, "The effect of MgO on the biodegradation, physical properties and biocompatibility of a Mg/HA/MgO nanocomposite manufactured by powder metallurgy method," *Journal of Alloys and Compounds*, vol. 655, pp. 266-280, 2016. https://doi.org/10.1016/j.jallcom.2015.09.107

[29] M. M. Castro *et al.*, "Magnesium-based bioactive composites processed at room temperature," *Materials*, vol. 12, no. 16, p. 2609, 2019. https://doi.org/10.3390/ma12162609

[30] J. Su, J. Teng, Z. Xu, and Y. Li, "Corrosion-wear behavior of a biocompatible magnesium matrix composite in simulated body fluid," *Friction*, vol. 10, no. 1, pp. 31-43, 2022. https://doi.org/10.1007/s40544-020-0361-8

[31] D. Z. Shamami, S. M. Rabiee, and M. Shakeri, "Characterization of magnesium-hydroxyapatite functionally graded composites prepared by rapid microwave sintering technique," *Ceramics International*, vol. 48, no. 9, pp. 12641–12653, 2022. https://doi.org/10.1016/j.ceramint.2022.01.133

[32] M. Casas-Luna *et al.*, "Degradable magnesium-hydroxyapatite interpenetrating phase composites processed by current assisted metal infiltration in additive-manufactured porous preforms," *Journal of Magnesium and Alloys*, vol. 10, no. 12, pp. 3641-3656, 2022. https://doi.org/10.1016/j.jma.2022.07.019

[33] M. Kasaeian-Naeini, M. Sedighi, R. Hashemi, and H. Delavar, "Microstructure, mechanical properties and fracture toughness of ECAPed magnesium matrix composite reinforced with hydroxyapatite ceramic particulates for bioabsorbable implants," *Ceramics International*, vol. 49, no. 11, pp. 17074-17090, 2023. https://doi.org/10.1016/j.ceramint.2023.02.069

[34] L. Drotárová *et al.*, "Biodegradable WE43 Mg alloy/hydroxyapatite interpenetrating phase composites with reduced hydrogen evolution," *Bioactive Materials*, vol. 42, pp. 519-530, 2024. https://doi.org/10.1016/j.bioactmat.2024.08.048

[35] A. B. Podgorbunsky *et al.*, "Bioresorbable composites based on magnesium and hydroxyapatite for use in bone tissue engineering: Focus on controlling and minimizing corrosion activity," *Ceramics International*, vol. 51, no. 1, pp. 423-436, 2025. https://doi.org/10.1016/j.ceramint.2024.11.016

© 2026 AESS Publications. All Rights Reserved.

[36] R. Acharya *et al.*, "3D-printed magnesium/nanodiamond dual-doped hydroxyapatite composite hydrogels with antibacterial and in vitro bioactive properties for bone tissue engineering," *Journal of the American Ceramic Society*, vol. 108, no. 12, p. e70121, 2025. https://doi.org/10.1111/jace.70121

[37] C. C. Narayanappa, B. Nagappan, P. Vignesh, and A. Thirugnanasambandam, "Assessment of biodegradability and biocompatibility: An experimental and comparative analysis of magnesium and magnesium-(zinc-tin)/hydroxyapatite composites," *Proceedings of the Institution of Mechanical Engineers, Part L: Journal of Materials: Design and Applications*, vol. 239, no. 5, pp. 1000–1012, 2024. https://doi.org/10.1177/14644207241270799

[38] F. Mansfeld, *The polarization resistance technique for measuring corrosion currents. In: M. G. Fontana, R. W. Staehle, ed. "Advances in corrosion science and technology.* New York: Plenum Press, 1976.

[39] T. Kokubo and H. Takadama, "How useful is SBF in predicting in vivo bone bioactivity?," *Biomaterials*, vol. 27, no. 15, pp. 2907–2915, 2006. https://doi.org/10.1016/j.biomaterials.2006.01.017

[40] ASTM Standard G31-72, *Standard practice for laboratory immersion corrosion testing of metals.* West Conshohocken, PA: ASTM International, 2004.

[41] S. Thomas, N. Kalarikkal, and A. R. Abraham, *Micro and nano technologies, design, fabrication, and characterization of multifunctional nanomaterials.* Amsterdam, Netherlands: Elsevier, 2022.

[42] K. E. Siva and G. Suresh, "Bioactive titanium-hydroxyapatite composites by powder metallurgy route," *Bioactive Research in Applied Chemistry*, vol. 12, no. 4, pp. 5375–5383, 2022. https://doi.org/10.33263/BRIAC124.53755383

[43] C. Chun, L. Chih-Te, C. Shih-Hsun, and O. Keng-Liang, "Effect of hydroxyapatite on the mechanical properties and corrosion behavior of Mg-Zn-Y alloy," *Materials*, vol. 10, no. 8, p. 855, 2017. https://doi.org/10.3390/ma10080855

[44] S. Jaiswal, R. M. Kumar, P. Gupta, M. Kumaraswamy, P. Roy, and D. Lahiri, "Mechanical, corrosion and biocompatibility behaviour of Mg-3Zn-HA biodegradable composites for orthopaedic fixture accessories," *Journal of the Mechanical Behavior of Biomedical Materials*, vol. 78, pp. 442–454, 2018. https://doi.org/10.1016/j.jmbbm.2017.11.030

[45] S. N. H. Abbas, H. Jafari, and A. Sadeghzadeh, "Investigating the corrosion behavior of biodegradable Mg–5Zn alloy coated with hydroxyapatite reinforced composite fabricated by friction stir process," *Journal of Materials Research and Technology*, vol. 29, pp. 5198–5213, 2024. https://doi.org/10.1016/j.jmrt.2024.02.162

[46] B. P. Chakraborty, S. Al-Saadi, L. Choudhary, S. E. Harandi, and R. Singh, "Magnesium implants: Prospects and challenges," *Materials*, vol. 12, no. 1, p. 136, 2019. https://doi.org/10.3390/ma12010136

[47] F. Liu, Y. Ji, Z. Sun, J. Liu, Y. Bai, and Z. Shen, "Enhancing corrosion resistance and mechanical properties of AZ31 magnesium alloy by friction stir processing with the same speed ratio," *Journal of Alloys and Compounds*, vol. 829, p. 154452, 2020. https://doi.org/10.1016/j.jallcom.2020.154452

[48] E. Gerashi, R. Alizadeh, and T. G. Langdon, "Effect of crystallographic texture and twinning on the corrosion behavior of Mg alloys: A review," *Journal of Magnesium and Alloys*, vol. 10, no. 2, pp. 313–325, 2022. https://doi.org/10.1016/j.jma.2021.09.009

[49] R. Krishnan *et al.*, "Biodegradable magnesium metal matrix composites for biomedical implants: synthesis, mechanical performance, and corrosion behavior–a review," *Journal of Materials Research and Technology*, vol. 20, pp. 650-670, 2022. https://doi.org/10.1016/j.jmrt.2022.06.178

[50] P. N. Lim, R. N. Lam, Y. F. Zheng, and E. S. Thian, "Magnesium-calcium/hydroxyapatite (Mg-Ca/HA) composites with enhanced bone differentiation properties for orthopedic applications," *Materials Letters*, vol. 172, pp. 193–197, 2016. https://doi.org/10.1016/j.matlet.2016.03.005

Views and opinions expressed in this article are the views and opinions of the author(s), Journal of Asian Scientific Research shall not be responsible or answerable for any loss, damage or liability etc. caused in relation to/arising out of the use of the content.

© 2026 AESS Publications. All Rights Reserved.